Construction and Building Materials 533 (2026) 146709

Contents lists available at ScienceDirect

Construction and Building Materials

journal homepage: www.elsevier.com/locate/conbuildmat

In-plane repair and strengthening of rubble stone masonry with single-sided natural hydraulic lime fabric reinforced mortar

Giovanni Sommacal [a], Ermes Rizzi [a], Jason Ingham [b,1], Ivan Giongo [a,*,2]

[a] Department of Civil, Environmental and Mechanical Engineering, University of Trento, via Mesiano 77, Trento 38123, Italy
[b] Department of Civil & Environmental Engineering, University of Auckland, Private Bag 92019, Auckland 1010, New Zealand

ARTICLE INFO

Keywords:
Stone masonry
Reinforcement techniques
Composite reinforced mortar (CRM)
Single-sided reinforcement
Natural hydraulic lime-based mortar
Diagonal compression test

ABSTRACT

Composite reinforced mortar (CRM) systems represent a strengthening solution for existing masonry structures consisting of a composite mesh embedded within a layer of structural mortar. Diagonal compression tests on natural stone masonry panels (URM) are reported, aimed at assessing the effectiveness of a hybrid CRM-FRCM system. The tested system was comprised of a 25 mm natural hydraulic lime-based mortar and a 20 × 20 mm AR glass grid applied on only one side of the panels in order to simulate the most commonly encountered strengthening configuration. The results showed an average increase in shear resistance of 32% compared to the average properties of the URM walls, while preserving the average shear stiffness. In addition, previously tested natural stone URM panels were repaired using the same strengthening solutions and were retested in diagonal compression. For the retested specimens the original shear capacity was recovered up to 98%, demonstrating the effectiveness of the strengthening system as a remediation solution for damaged masonry.

1. Introduction

Unreinforced masonry (URM) buildings dominate the existing building stock in many countries worldwide, with specific masonry characteristics and construction practices often varying greatly even within a single country. Despite this variability, a common trait of URM buildings is a high vulnerability to seismic loading [1–6], with out-of-plane wall failures being characterised as a local failure mechanism [7] whereas the overall seismic performance of a URM building is typically associated with the in-plane wall capacity [8]. Among the available in-plane strengthening solutions for URM walls, jacketing using various types of reinforced coatings has become increasingly popular as an efficient method to increase the in-plane seismic capacity by improving both the strength and deformation capacity of existing masonry piers and spandrels [9–12].

Concrete jacketing reinforced with welded steel mesh (also known as ferrocement jacketing) has been extensively used to strengthen masonry since the early 1980s [13–15], endorsed in Italy by codes drafted in the aftermath of the 1976 Gemona earthquake and the 1980 Irpinia earthquake [16]. The thickness of the concrete jacket usually varies from 40 mm to 70 mm such that the reinforced concrete jacketing results in a significant increase in the wall mass and stiffness, which may adversely affect the seismic behaviour of the overall masonry structure [17–19]. Moreover, the application of this technique involves other disadvantages such as a possible reduction of available floor plan area, the potential for steel corrosion (with associated loss of capacity and volume instability) and most notably a lack of reversibility [8,20,21].

Following the development of composite materials the practice of concrete jacketing has been partially replaced by the adoption of *Fibre-Reinforced Polymer* (FRP) as a retrofit solution [18,21,22], combining various organic matrices with glass, aramid or carbon fibres. Guidelines for the application of these techniques are available for the process of identification and qualification [23] and for design [24,25]. FRP solutions have proven to be highly effective in enhancing shear resistance [26–30] and offer several advantages over traditional retrofitting material, including a large strength to weight ratio, a faster installation rate and a reduced plaster thickness (between 2 mm and 5 mm) [31]. However, the application of FRP as a URM jacketing solution also has some important drawbacks, such as poor compatibility with the substrate, lack of vapour permeability, the need for expert craftmanship

* Corresponding author.
E-mail addresses: giovanni.sommacal@unitn.it (G. Sommacal), ermes.rizzi@unitn.it (E. Rizzi), j.ingham@auckland.ac.nz (J. Ingham), ivan.giongo@unitn.it (I. Giongo).
[1] ORCID number: 0000-0002-0989-909
[2] ORCID number: 0000-0002-3867-2334

https://doi.org/10.1016/j.conbuildmat.2026.146709
Received 2 May 2025; Received in revised form 10 May 2026; Accepted 12 May 2026
Available online 23 May 2026

and, again, the lack of reversibility [21,32,33]. Many of these problems are related to the use of epoxy resins applied to impregnate the reinforcing fibres.

The above issues may be overcome by using more modern composite jackets, made by placing reinforcement meshes in an inorganic matrix consisting of either lime-based or cement-based mortars. These solutions combine high mechanical performance with the equally important features of sustainability and durability. Furthermore, the use of high-performance lime-based mortars [34] to provide the matrix of the composite ensures a high level of compatibility between the inorganic jacket and the masonry surface, resulting in an effective solution for historical masonry structures [20,32,35–38] and these lime-based inorganic-matrix composite materials can be removed with relative ease, guaranteeing reversibility of the solution [39]. These systems are categorized into two different groups according to their jacket thickness and mesh grid spacing, named *Fabric Reinforced Cementitious Matrix* (FRCM) and *Composite Reinforced Mortar* (CRM). Both systems can be applied in either a single-sided or double-sided configuration, with the double-sided configuration being more efficient in terms of enhancing resistance but the single-sided configuration frequently being preferred because of the practical challenges of providing a jacket to both wall surfaces [40].

FRCM solutions are also sometimes referred to as *Textile Reinforced Mortar* (TRM) [37,41–43] or *Textile Reinforced Concrete* (TRC) [44,45], and consist of a relatively thin jacket that combines medium-high performance mortars with FRP meshes generally made of *Akali Resistant* (AR) glass, basalt, carbon or aramid fibres. High-performance steel cords can also be embedded in the inorganic mortar, in which case the system is usually named *Steel Reinforced Grout* (SRG) [46]. When the reinforcing meshes are replaced by steel fibers randonmly spread in the mortar, the system is referred to as *Steel Fiber Reinforcing Mortar* SFRM [47]. The randomly distributed fibers can also be made of basalt or glass, in which case the system is referred to as BFRM or GFRM, respectively [48]. Hybrid configurations have also been investigated, consisting of TRM systems with an inorganic matrix modified with short PVA fibers [49–51]. Returning to FRCM systems, which in some cases are also referred to as FRM [52] the reinforcement grids are characterized by a reduced thickness and by a spacing of less than 30 mm. The thickness of the composite may vary depending on the number of layers [53] and the textile used, but when a single layer of mesh is employed the FRCM system has a thickness of between 5 mm and 15 mm whereas when more than two layers are used the thickness can reach 30 mm. The use of mechanical anchorages is not always mandatory, but it is mandatory for an asymmetrical configuration [54]. For these reasons FRCM applications can be compared with FRP applications, with specific identification and qualification [55,56] and design [57,58] guidelines for FRCM systems.

CRM techniques are high thickness strengthening solutions that combine a 30–50 mm thickness mortar matrix with only one layer of mesh reinforcement, usually manufactured using AR-glass fibres embedded in epoxy resin [59–63]. This type of grid typically presents a larger wire cross section than used in FRCM solutions and has a spacing of at least 30 mm, with the provision of mechanical connectors being mandatory. CRM solutions can be considered as a substitute for traditional ferrocement jacketing of masonry structures. For CRM only identification and qualification guidelines are available in Italy [64] and in Europe [65] to date. Therefore, according to the current design codes, for their design it is necessary to refer to the simplified approach proposed by the application document for the current *Italian Building Code* (Circolare n.7 2019) [66]. Nevertheless, analytical prediction models for TRM systems incorporating the contribution of the mortar layer have also been proposed in the literature [67,68].

FRCM solutions are characterised by a reduced footprint and a small mass increase because of their reduced jacket thickness, and when no mechanical connectors are used these jackets require a low labour input. However, FRCM plasters are generally less suitable for application on irregular masonry surfaces, even though examples of successful applications to masonry panels with irregular textures are available in the literature [38,69], because of the difficulty in achieving a thin, uniform levelling layer over an uneven substrate. Conversely, due to the concurrent presence of a more consistent matrix and a stiffer grid combined with a greater jacket thickness, CRM plasters are ideal for reinforcing irregular masonry [39] but they can become more expensive because of their perforations and the installation of the required anchorages.

While recent research has provided in-depth experimental and numerical insights into the performance of double-sided FRCM systems applied to stone masonry [38], there remains a need to investigate asymmetrical configurations and the effectiveness of such systems for the repair of pre-damaged elements. In the present work the mechanical behaviour of stone masonry panels strengthened with an asymmetrical hybrid CRM-FRCM reinforcing plaster solution made of a flexible GFRP grid embedded in a 25 mm lime-based mortar thickness was experimentally investigated. The CRM jacket system was adopted due to its suitability for application on the irregular surfaces typical of stone masonry. However, since the experimental campaign was undertaken in 2019, prior to the official release of standardised procedures [64,65], the adopted system did not comply with the Italian Guidelines for CRM systems [64]. In particular, the jacket thickness of 25 mm was below the minimum threshold of 30 mm, the fabric grid spacing of 20 mm was smaller than the required 30 mm, and the connectors used were made of steel rather than FRP, as specified in the qualification guidelines [64, 65], which were not yet available at the time the testing campaign was planned and executed. The reduced nominal thickness is not expected to have significant technical implications, as substrate irregularity results in an average reinforcement thickness within the limits defined in [64]. Although the denser thread distribution may improve the mesh effectiveness against diagonal cracking, the overall geometrical and mechanical properties (tensile strength per unit width and elastic modulus of the mesh, reinforcement thickness over mesh width ratio) are comparable to those of typical CRM system. For this reason and for the sake of brevity, the investigated strengthening solution will be referred to as a CRM system in the subsequent sections. In-plane diagonal tests were undertaken on both unreinforced and reinforced panels to establish the effectiveness of the reinforcement in term of shear strength and stiffness and energy dissipation. CRM was applied on only a single face of the wall to simulate a common practical application scenario that is less reported in the scientific literature. The use of a natural hydraulic lime-based mortar provided maximum compatibility with the wall surface. The reported study provides an important contribution to the scientific community by complementing existing experimental data for FRCM/CRM systems applied to stone masonry via the provision of experimental data for asymmetrical configurations for both strengthening and repair scenarios.

2. Experimental program

The purpose of the reported experimental campaign was to assess the effectiveness of a single-sided CRM system applied on rubble stone masonry wallettes. The campaign comprised a series of diagonal tension (shear) tests carried out according to the general procedure outlined in ASTM E519/E519M-15 [70]. A total of 12 tests were performed on eight 1200×1200 mm^2 $\times$ 400 mm-thick double-leaf rubble stone masonry wallette panels that were built by expert craftmanship. The specimen thickness was compliant with the limitations proposed in NTC18 [71], which sets the lower bound for the thickness of structural masonry as equal to 240 mm. Despite being a rather common typology in traditional buildings, the selected masonry type has rarely been investigated in previous experimental works. The eight masonry wallettes were identified by means of numerical labels and subdivided into 2 groups of four specimens each, named Group 1 and Group 2. Group 1 wallettes were first tested in the as-built (*AsB*) configuration, and then the CRM system was applied to the damaged Group 1 wallettes and the wallettes were subsequently re-tested in the repaired (*RP*) condition, being representative of a scenario where the CRM system is applied to an existing masonry structure that was previously damaged, with the aim of restoring the original mechanical properties of the wall. Group 2 specimens were tested in the *RT* (retrofitted) configuration only. All specimens were tested shortly after the 28-day mortar curing time had elapsed, with test designations identified in Table 1.

3. Materials

The masonry wallettes were assembled using approximately square dolomite stone blocks and natural hydraulic lime mortar. Dolomite stone (also known as dolostone) is a sedimentary carbonate rock that contains high percentages of dolomite mineral and typically features a light grey colour with brown veins. The stone elements were roughly squared by means of manual tools, resulting in blocks of variable sizes. The average maximum dimension of the blocks was approximately 250 mm, with values ranging between 100 mm and 400 mm. The resulting masonry texture was irregular, as shown in Fig. 1.

The mechanical properties of the stone elements were not investigated within the scope of the experimental campaign. However, according to ASTM C568/C568M-15 [72] and C170/C170M-17 [73] the compressive strength of limestone blocks ranges between 11 MPa and 220 MPa, whilethe compressive strength of dolomite masonry units typically ranges between 59 MPa and 196 MPa [74].

The bedding mortar used to assemble the wallette specimens was an M 2.5 strength class NHL 5 Portland cement-free natural hydraulic lime mortar, CE marked according to EN 998–2 [75]. This pre-mixed mortar contained aggregates obtained via the crushing of dolomite stones, with a maximum particle size of 2 mm, and was mixed with water according to the technical data sheet. The specific mortar was selected to reproduce the mechanical properties of mortars that can be found in existing buildings in terms of both the type of binder and the relatively low compressive strength. The actual mechanical properties of the mortar were determined in accordance with EN 1015–11:2019 [76] based on the results of testing carried out as specified in the standard (see Fig. 2). A total of six 40 × 40 × 160 mm^3 mortar prisms were prepared and tested after 28 days of curing, with an average flexural strength of $f_{bedding\ m,m}$ = 1.73 MPa (6 tests, COV = 6.02%) and an average compressive strength of $f_{bedding\ m,c}$ = 5.40 MPa (12 tests, COV = 7.36%). The tested CRM system consisted of a GFRP mesh embedded in a 25 mm-thick layer of NHL 5 natural hydraulic lime mortar that was connected to the substrate by means of helical stainless-steel dowels, applied as illustrated in Fig. 3. The helical dowels were fixed to the masonry substrate using a specific inorganic grout composed of NHL 5 hydraulic lime binder and fine dolomitic aggregates (maximum particle size < 0.5 mm), with a compressive strength after 28 days of curing greater than 15 MPa, according to [76]).

The selected grid fabric was a balanced bidirectional fabric made of alkali-resistant glass fibres coated with a protective thermosetting resin (GFRP) (Fig. 3), with a centre-to-centre grid spacing equal to 20 mm for both warp and weft directions (clear grid opening equal to 18 mm). The main geometrical and mechanical proprieties of the grid fabric according to the technical data sheet are listed in Table 2, with data reported separately for the ultimate tensile strength f_t and the ultimate tensile strain ε_t based on the procedures used to determine the reference value in North America (ACI, mean minus one standard deviation) and Europe (RILEM CNR, mean minus one fractile coefficient times the standard deviation, where the fractile coefficient depends on the number of tested specimens [77]). Mechanical parameters in Table 2 are related to test methods compliant with the procedures outlined in [55,56]. A sample of six fabric specimens was also tested to verify the values provided by the manufacturer, confirming a linear elastic response up to failure ($\langle ft \rangle$ = 940 MPa, CoV = 3.8%; Et = 64657 MPa, CoV = 1.5%; $\langle \varepsilon t \rangle$ = 1.43%, CoV = 3.3%).

The mortar used for the CRM system was a pre-mixed M10 strength class Portland cement-free NHL 5 natural hydraulic lime mortar with dolomitic aggregates (maximum particle size 4 mm), CE marked according to EN 998–2 [75]. The manufacturer's documented ranges for the mix proportions by weight were: binder 15–25%; aggregate 75–85%, mixing water 145–155 g/kg. The mortar was selected with the aim of maximizing the compatibility-related aspects of the CRM system. Natural hydraulic lime mortars are typically characterized by mechanical and chemical features that are comparable with those of the existing mortars, which are mostly lime-based binders. Furthermore, the modulus of elasticity (stiffness) of hydraulic lime-based mortars is generally lower than for cement-based mortars, especially in the case of relatively low strength classes [78]. The actual mechanical properties of the mortar were assessed according to EN 1015–11:2019 [76], with a total of six 40 × 40 × 160 mm^3 mortar prisms prepared and tested after 28 days of curing. The average flexural strength was equal to $f_{matrix\ m,m}$ = 3.41 MPa (6 tests, COV = 8.32%) and the average compressive strength was $f_{matrix\ m,c}$ = 13.95 MPa (12 tests, COV = 16.98%).

Although composite coupons (i.e., small lamella specimens composed of mesh slices embedded in mortar) were not prepared and tested in this study, twenty 10 mm-thick coupons made of the same grid fabric and an M15 lime–cement mortar were tested in a parallel study according to FRCM composite procedures, and the corresponding values are reported in Table 3.

The same study also comprised 5 shear bond tests on stone masonry using the same composite specifications mentioned in the previous paragraph (same grid fabric and M 15 lime-cement mortar, composite thickness 10 mm) as reported in Table 3. The results from these shear bond tests are reported in Table 4. The values reported in Table 3 and in Table 4 were adopted for the composite in the comparisons with codes provisions reported in the following, whilst recognising that the results were derived for a similar but different mortar classification and composite thickness.

The connection system comprised Ø8 mm helical *AISI 304* stainless steel bars (see Fig. 3) housed into Ø20 mm holes and fixed to the substrate by means of a specific NHL 5 natural hydraulic lime grout. The main geometrical and mechanical properties of the steel bars according to the technical data sheet are listed in Table 5.

The CRM system was applied on a single side of all masonry wallettes using five mechanical connectors per specimen (approximately equivalent to 4 connections/m^2) in accordance with the manufacturer recommendations and consistently with comparable studies in the literature (e.g., [59,79]). The overall thickness of the CRM system was equal to 25 mm, net of substrate levelling. The strengthening procedure is summarized in the following steps:

1. Drilling of the five Ø20 mm, 300 mm-deep connector housing holes (3/4 of the masonry thickness) inclined at approximately 30° with respect to the horizontal (see Fig. 4-a). Four holes were located at the specimen corners (respecting a minimum distance of 250 mm from the edges) and one hole was drilled at the centre of the specimen. Holes were subsequently cleaned from drilling residuals by means of

Table 1
Test designation details.

Configuration	Test ID	Wall ID
As-built	*AsB-1*	1
	AsB-2	2
	AsB-3	3
	AsB-4	4
Repaired	*RP-1*	1
	RP-2	2
	RP-3	3
	RP-4	4
Retrofitted	*RT-1*	5
	RT-2	6
	RT-3	7
	RT-4	8

(a) Wallette construction phase *(b) Finished wallette*

Fig. 1. Details of rubble stone masonry wallettes.

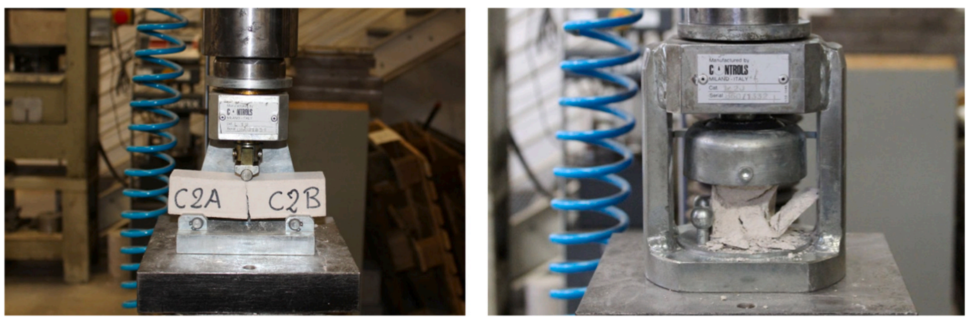

(a) (b)

Fig. 2. Testing of mortar prisms according to EN 1015–11:2019: a) 3-point bending test; b) Compression test.

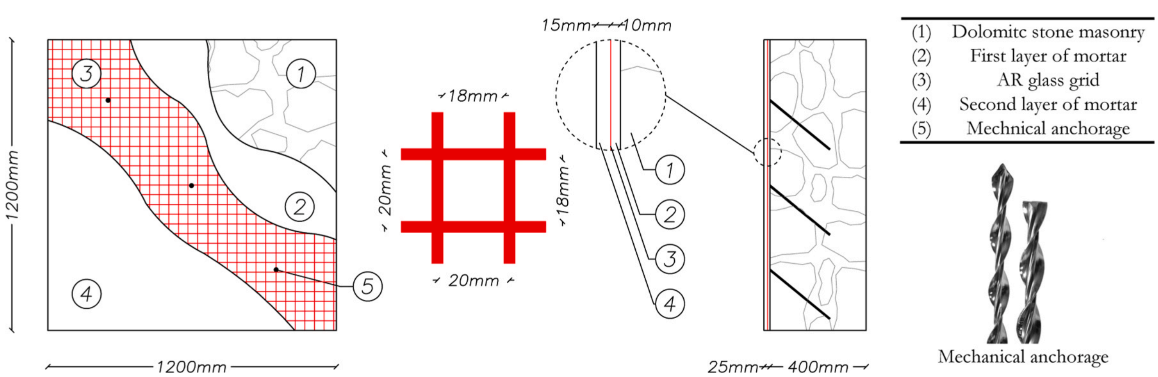

Fig. 3. Details of the strengthening solution.

compressed air. The adopted quincunxes connection scheme was selected in order to have a minimum centre-to-centre connector distance of 50 cm while providing sufficient distance from the edges of the wallette;

2. Gravity injection of the NHL 5 natural hydraulic lime grout within the connector housing holes until completely filled (see Fig. 4-b);
3. Insertion of the helical steel dowels in the holes, dipping them into the still fluid grout injected during the previous step. Dowels were inserted so that a 100 mm-long portion protruded from the hole;
4. Preparation of the masonry substrate by means of cleaning and pre-wetting with low-pressure water until saturation;
5. Application of the first layer of mortar, for a thickness of approximately 15 mm net of substrate levelling;
6. Positioning of the mesh in the still workable first layer of mortar by applying a slight pressure. Principal directions of the mesh were aligned with the specimen edges such that the warp wires were laid vertically and weft wires were oriented in the horizontal direction. Wallette specimen dimensions required two mesh slices per specimen, overlapping them for 150 mm (see Fig. 4-c);
7. L-folding over the mesh of the protruding portion of the helical dowels;
8. Application of the second and final layer of mortar, up to an overall thickness of 25 mm net of substrate levelling (see Fig. 4-d).

Four specimens (*AsB* group) were first tested in the unreinforced as-built condition and then repaired and retested to investigate the use of this solution on damaged structures. For this group of repaired samples (*RP* group) the reinforcing procedure was applied using the same procedure as was adopted for the retrofitted (*RT* group) specimens.

Table 2
Geometrical and mechanical proprieties of the grid fabric.

Horizontal direction (weft)		Single wire cross section area	[mm^2]	0.9981
		Equivalent thickness, t_{fH}	[mm]	0.046
		Tensile modulus of elasticity (stiffness), E_t	[MPa]	63057
		Ultimate tensile strength (mean), $\langle f_t \rangle$	[MPa]	882
		Ultimate tensile strain (mean), $\langle \varepsilon_t \rangle$	[%]	1.39
	ACI	Ultimate tensile strain (reference), ε_{tk}	[%]	1.63
	RILEM	Ultimate tensile strength (reference), f_{tk}	[MPa]	574
	& CNR	Ultimate tensile strain (reference), ε_{tk}	[%]	0.91
Weight density		Dry fabric	[g/m^2]	240
		Coated fabric	[g/m^2]	320

Table 3
Mechanical proprieties of the composite.

	Tensile modulus of elasticity (stiffness), E_f	[MPa]	28491
	Mean ultimate tensile strength, $\langle f_{fu} \rangle$	[MPa]	603
	Mean ultimate tensile strain, $\langle \varepsilon_{fu} \rangle$	[%]	1.91
ACI	Design tensile strain, ε_{fd}	[%]	1.25
CNR	Characteristic ultimate tensile strength, σ_u	[MPa]	425

Table 4
Results from shear bond tests.

	Mean maximum tensile stress, $\langle f_{fb} \rangle$	[MPa]	813
	Mean maximum tensile strain, $\langle \varepsilon_{fb} \rangle$	[%]	1.29
RILEM & CNR	Characteristic maximum tensile strain, ε_{fb} ($\varepsilon_{\lim,conv}$ for CNR)	[%]	0.73

Table 5
Geometrical and mechanical proprieties of the mechanical anchorages.

Gross diameter	[mm]	8
Core diameter	[mm]	4
Cross sectional area	[mm^2]	10.40
Tensile strength	[MPa]	1067
Young's modulus	[MPa]	122000

4. Test setup and protocol

Diagonal tension (shear) tests were carried out following the general procedure outlined in ASTM E519/E519M-15 [70], which is a laboratory test procedure that has been widely reported for experimentally assessing the in-plane shear strength of masonry walls [80]. Diagonal compression tests are also mentioned in NTC18 [71] as one of a series of exhaustive tests that can be performed on masonry elements. A self-equilibrated test setup was designed to allow the test to be executed without rotating the specimens, as illustrated in Fig. 5. The diagonal compression load was applied via a manually operated hydraulic jack with a maximum capacity of 600 kN (Fig. 5(c)). The jack was positioned between the steel beam and the steel shoe at the upper loaded corner of the specimen. The load was transferred by the upper steel beam to the two threaded steel bars that reacted off the steel beam connected to the steel shoe at the lower loaded corner (Fig. 5(e)). Applied load was measured via a 600 kN load cell interposed between the hydraulic jack and the steel beam at the upper loaded corner. As also suggested by ASTM E519/E519M-15 [70], the stress distribution on the loaded portions was improved by laying an approximately 20 mm-thick layer of M 15 strength class mortar over the loaded corners. Four 100 mm displacement transducers were installed along the two diagonals, two on each face of the wall, to measure the tensile and compressive displacements. The specimens were tested under force control, with the diagonal compression load applied using a manual pump in stepped cycles of loading and unloading, each with an amplitude of approximately 50 kN. For all specimens, an initial loading cycle was carried out at a lower value (25 kN) to ensure proper seating of the steel shoes in their correct positions. Due to the irregularity of the masonry surfaces the application of these four devices required the use of square wood blocks to generate a flat surface on which to install the instrumentation (Fig. 5(f)). No system was implemented to restrain potential out-of-plane movements of the wallette, which evidence in the literature has shown can be significant in the presence of asymmetrical reinforcement [65–67]. During testing, particular care was therefore taken to visually monitor the verticality of the panel.

5. Test results and discussion

Test results were compared based on a series of parameters representative of shear strength, shear stiffness, inelastic deformation capacity and symmetry of structural response, with the values of the shear stress τ_m, shear strain γ and shear modulus G being calculated according to ASTM E519/E519M-15 [70]. The shear stress was computed using Eq. (1) where P is the applied compression load and A_n is the net specimen cross sectional area calculated according to Eq. (2) in which w, h, and t are the width, the height, and the thickness of the specimen, respectively. For the repaired and retrofitted specimens the thickness increment related to the CRM system was neglected and stresses were calculated with respect to the unreinforced specimen cross-sectional area. Due to the masonry texture irregularities, nominal values of the geometrical properties were used in the calculations.

$$\tau = \frac{0.707 \bullet \mathrm{P}}{\mathrm{A_n}} \tag{1}$$

$$\mathrm{A_n} = \left(\frac{\mathrm{w}+\mathrm{h}}{2}\right) \bullet \mathrm{t} \tag{2}$$

Average axial strain along the compression and the tensile diagonals ($\varepsilon_{C,mean}$ and $\varepsilon_{T,mean}$, respectively) were calculated by averaging the strain readings of the relevant transducers on the opposite sides of the specimens. The average shear strain γ was calculated from $\varepsilon_{C,mean}$ and $\varepsilon_{T,mean}$ values according to Eq. (3).

$$\gamma = |\varepsilon_{\mathrm{C,mean}}| + |\varepsilon_{\mathrm{T,mean}}| \tag{3}$$

The shear modulus G is defined as the ratio between the shear stress and the shear strain as per Eq. (4).

$$\mathrm{G} = \frac{\tau}{\gamma} \tag{4}$$

To provide shear stiffness values representative of the initial branch of the shear stress vs strain diagrams the secant shear modulus G_{el} was evaluated. This parameter is usually computed as the ratio between the shear stress and the corresponding shear strain at one-third of the peak shear strength as suggested by NTC18 [71], but in this study the definition of the secant shear modulus was modified to be more representative of a bilinear elastic-perfectly plastic response. Specifically, the shear modulus was calculated between 5% and 75% of the shear capacity of the individual test as per Eq. (5), in which $\gamma_{5\%}$ and $\gamma_{75\%}$ are the shear strain calculated according to Eq. (3) for a load level corresponding to $0.05F_{max}$ and $0.75F_{max}$, respectively:

$$G_{el} = \frac{0.75 \bullet \tau_{\max} - 0.05 \bullet \tau_{\max}}{\gamma_{75\%} - \gamma_{5\%}} \tag{5}$$

The shear stress vs shear strain curves were bi-linearized according to the procedure outlined in ASTM E2126–19 [81] (referred to as

Fig. 4. Strengthening procedure: a) drilling of inclined holes; b) manual injection of the anchoring grout; c) first layer of mortar and.

Fig. 5. Test set-up details.

Equivalent Energy Elastic-Plastic curve or EEEP), with cyclic curves firstly enveloped by connecting the peak force points for each of the subsequent load cycles and the slope G_{el} calculated as described above. To provide consistent values for yield stress and yield strain the envelope curves were truncated at the point corresponding to a pre-defined loss of applied load ($0.90F_{max}$) on the post-peak branch of the envelope curves, identifying the ultimate shear strain γ_u. The yield strain γ_y and yield stress τ_y ($= G_{el} \times \gamma_y$) were calculated by preserving the area (energy) under the envelope curve and the equivalent bilinear curve. The specific energy dissipation En_{dis} was calculated as the area below the EEEP diagram plateau.

The asymmetry index I_A was defined according to Eq. (6) to assess the symmetry of the in-plane behaviour of the specimens, where $\varepsilon_{C,L}$ and $\varepsilon_{C,R}$ are the measured strains along the compressed diagonal on the left side and the right side of the specimens, respectively. A near-zero asymmetry index is reported for a symmetric wall response ($\varepsilon_{C,L}$=$\varepsilon_{C,R}$), with a greater deviation from symmetrical behaviour resulting in a greater asymmetry index.

$$\mathrm{I_A} = |\varepsilon_{\mathrm{C,R}} - \varepsilon_{\mathrm{C,L}}| \tag{6}$$

The cyclic diagram obtained directly from each diagonal compression test, the envelope curve, and the EEEP bi-linearization are reported in Fig. 6, Fig. 7 and Fig. 8. For each tested configuration the specimens exhibited an approximately linear response in the shear stress vs shear strain plane up to a load level approximately equal to 0.7 τ_{max}. Subsequently, crack propagation was visually detected and the shear stiffness gradually decreased. After the peak shear stress τ_{max} was reached the load application was switched to displacement control. For the repaired (*RP*) and retrofitted (*RT*) specimens, no rupture of the grid and no detachment of the reinforcement at the matrix-masonry interface were observed during testing, confirming the efficacy of the installation procedure reported earlier.

The experimental results are listed in Table 6, with symbols being consistent with the descriptions given in the previous paragraphs. Overall, the test results were generally consistent among analogous specimen configurations in terms of strength values, with the coefficient of variation (CoV) always below 15%. For instance, for the As-built set the coefficient of variation associated with the peak shear stress was 9%, which is well below the 24% value suggested by FprEN1998–3:2025 [82] for the diagonal tensile strength of irregular stone and rubble masonry. Conversely, the shear stiffness values obtained from the tests exhibited higher variability, with CoVs of 33% and 32% for the As-built and Retrofitted sets, respectively, compared with the 21% value recommended by FprEN1998–3:2025. The smaller variability observed for the Repaired set (CoV = 13%) is attributed to the predominant contribution of the CRM layer to the overall stiffness, due to the presence of pre-existing cracking in the masonry substrate.

The as-built (*AsB*) specimens exhibited a relatively linear elastic behaviour when subjected to in-plane diagonal compression, as shown in Fig. 6, and reached approximately consistent values of maximum shear stress, with an average value of 0.31 MPa. The asymmetry index is shown in Fig. 9, indicating that the asymmetry of the as-built specimens increased with increased loading due to the non-homogeneous nature of the panel texture. On both sides of each as-built (*AsB*) specimen the failure mode was governed by cracking that expanded along the compressed diagonal, located at the interface between stone units and the bed-joint mortar as shown in Fig. 10(a,d).

As shown in Fig. 7, the repaired (*RP*) wallettes exhibited an initial elastic shear stress vs shear strain behaviour, but with a reduced stiffness when compared to the as-built (*AsB*) wallettes. Despite the reinforced plaster was located on only one surface of the wallettes, comparable levels of the Asymmetry Index I_A were observed for consistent levels of shear strain. However, the increased shear strain capacity of the *RP* wallettes resulted in a corresponding increase in the Asymmetry Index that was approximately three times the peak value measured for the as-built (*AsB*) wallettes, as seen in Fig. 9(a). As shown in Fig. 10(e), distributed principal diagonal cracking formed in the CRM matrix, whilst on the unplastered (as-built) face the primary cracking developed along the same path as detected for the as-built specimens (see Fig. 10 (b)).

The retrofitted wallettes (*RT*) exhibited the same initial trend as for as-built (*AsB*) wallettes up to a shear stress level greater than that of the as-built specimens, indicating effective composite action between the masonry and the CRM system. Initial cracking was delayed by the presence of the reinforcement and maximum values of the asymmetry index were comparable to the values measured for the as-built specimens (see Fig. 9(b)). On the reinforced surface of the wallettes the presence of the CRM layer resulted in a crack pattern aligned with the applied load direction (see Fig. 10(f)), with a first principal crack along the compressed diagonal followed by several parallel secondary cracks. RT specimens generally showed a more distributed crack pattern than RP specimens, where crack localization was likely driven by the pre-existing substrate discontinuity, namely the diagonal crack formed during the AsB test sequence.

The mean *shear stress-strain* curves and the minimum–maximum envelope obtained from the individual experimental curves are reported in Fig. 11 to allow a visual assessment of the effectiveness of the applied CRM system. The comparison reported in Table 7 in terms of the Performance Ratio (*PR*) of the peak shear stress *PR*(τ_{max}) and of the shear modulus *PR*(G_{el}). For the repaired specimens the *PR* was calculated as the measured values for each repaired specimen divided by the comparable measured values for the corresponding as-built specimen, whereas for the retrofitted specimens the *PR* was calculated as the ratio of the measured value to the calculated average value of the four as-built specimens (see Table 6 for data). In Table 7 it is shown that the CRM system resulted in the shear strength of the repaired (*RP*) wallettes being restored to 98% of the capacity of the original as-built (*AsB*) wallettes, indicating that the matrix was effective at collaborating with the masonry substrate and compensating for the pre-existing cracks generated during testing of the *AsB* specimens. However, because of these pre-existing cracks the shear stiffness was significantly reduced to only 25% of the original value.

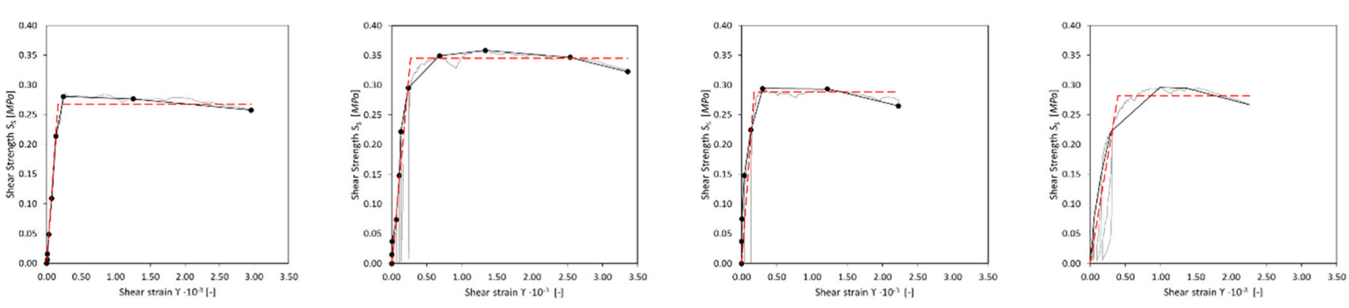

(a) AsB_01 (b) AsB_02 (c) AsB_03 (d) AsB_04

Fig. 6. Experimental shear stress-shear strain diagrams of the as-built wall specimens ("AsB" group).

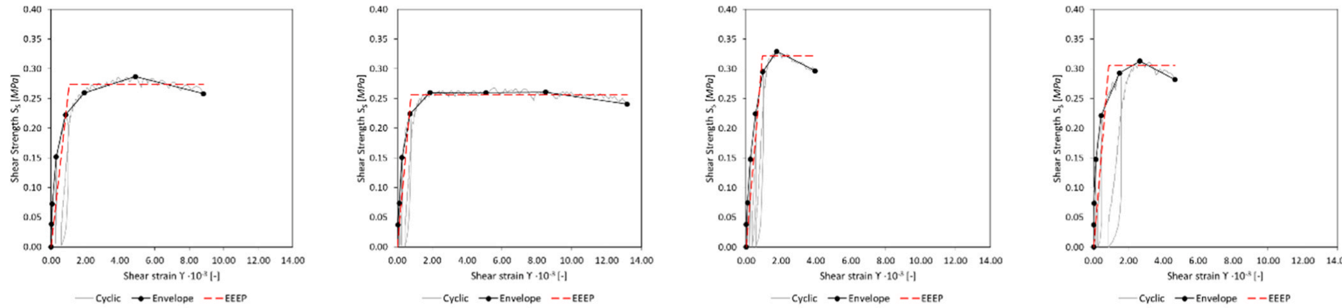

(a) RP_01 (b) RP_02 (c) RP_03 (d) RP_04

Fig. 7. Experimental shear stress-shear strain diagrams of the repaired wall specimens (“RP” group).

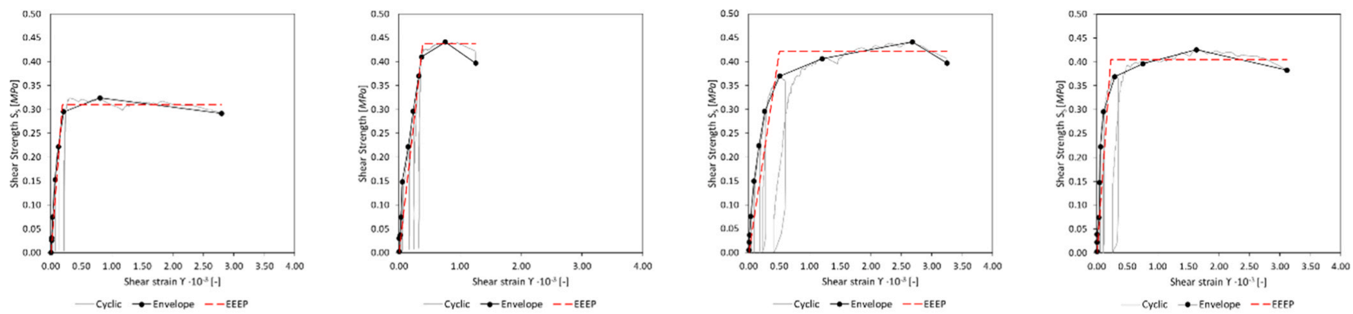

(a) RT_01 (b) RT_02 (c) RT_03 (d) RT_04

Fig. 8. Experimental shear stress-shear strain diagrams of the retrofitted wall specimens (“RT” group).

Table 6
Summary of the diagonal compression test results.

Group	Label	P_{max} [kN]	τ_{max} [MPa]	G_{el} [MPa]	$I_{A,max}$ [‰]	$\gamma_y \cdot x10^{-3}$ [-]	$\gamma_u \cdot x10^{-3}$ [-]	En_{dis} [kJ/m^3]
As-built	*AsB_01*	194.27	0.29	1606.74	1.69	0.166	2.959	746.33
	AsB_02	243.27	0.36	1275.52	1.28	0.271	3.359	1066.10
	AsB_03	199.64	0.29	1625.61	0.28	0.177	2.226	589.82
	AsB_04	201.00	0.30	713.79	1.91	0.394	2.266	526.78
	Average	**209.54**	**0.31**	**1305.42**	**1.29**	**0.25**	**2.70**	**732.26**
	C.O.V.	**0.11**	**0.11**	**0.33**	**0.56**	**0.42**	**0.20**	**0.33**
Repaired	*RP_01*	194.60	0.29	262.71	5.53	1.042	8.840	2134.44
	RP_02	181.50	0.27	329.73	4.06	0.778	13.158	3176.40
	RP_03	223.58	0.33	342.98	1.91	0.939	3.954	971.31
	RP_04	212.42	0.31	352.05	1.36	0.866	4.673	1160.99
	Average	**203.03**	**0.30**	**321.87**	**3.22**	**0.91**	**7.66**	**1860.78**
	C.O.V.	**0.09**	**0.09**	**0.13**	**0.60**	**0.12**	**0.56**	**0.55**
Retrofitted	*RT_01*	219.87	0.32	1617.59	1.63	0.191	2.798	805.69
	RT_02	299.48	0.44	1132.42	1.00	0.387	1.255	380.32
	RT_03	299.54	0.44	834.16	1.93	0.505	3.247	1155.38
	RT_04	288.84	0.43	1776.56	1.26	0.228	3.117	1170.29
	Average	**276.93**	**0.41**	**1340.18**	**1.45**	**0.33**	**2.60**	**877.92**
	C.O.V.	**0.14**	**0.14**	**0.32**	**0.28**	**0.44**	**0.35**	**0.42**

The retrofitted wallettes (*RT*) achieved a considerable increase of shear strength when compared to the as-built (*AsB*) wallettes, with the shear stiffness remaining relatively unchanged. These observations are confirmed in Table 7, showing that the retrofitted wallettes exhibited a mean increase in shear strength of 32%, with this value increasing to 41% if the abnormally low shear strength value of specimen *RT_01* is discounted. The observed shear strength increment was consistent with the results reported in literature (see Table 8) for single-sided lime-based CRM systems applied on irregular stone masonry [83] and on regular tuff masonry [59]. In [79] higher values are reported for a consistent hybrid CRM/FRCM strengthening system applied on rubble masonry specimens. It is worth noting that in [79] the diagonal compressive load directly engaged the reinforcement layer, rather than being applied solely on the masonry portion of the specimen, likely influencing the measured shear strength values. The negligible (3%) increase of shear stiffness is advantageous, overcoming the problem of significant stiffness increase that is routinely encountered when applying traditional reinforced plasters made with the use of cement mortars and steel mesh. This unaltered stiffness is highly beneficial, as it prevents problematic changes to the global force patterns, allowing for targeted strengthening of the most vulnerable piers without unintentionally attracting higher seismic demands. This outcome is primarily governed by the geometrical ratio of the intervention, with the CRM layer representing only 6% of the total wallette thickness. Additionally, the selection of a natural hydraulic lime (NHL) matrix ensures a degree of deformability that promotes compatibility with the stone masonry, avoiding the excessive

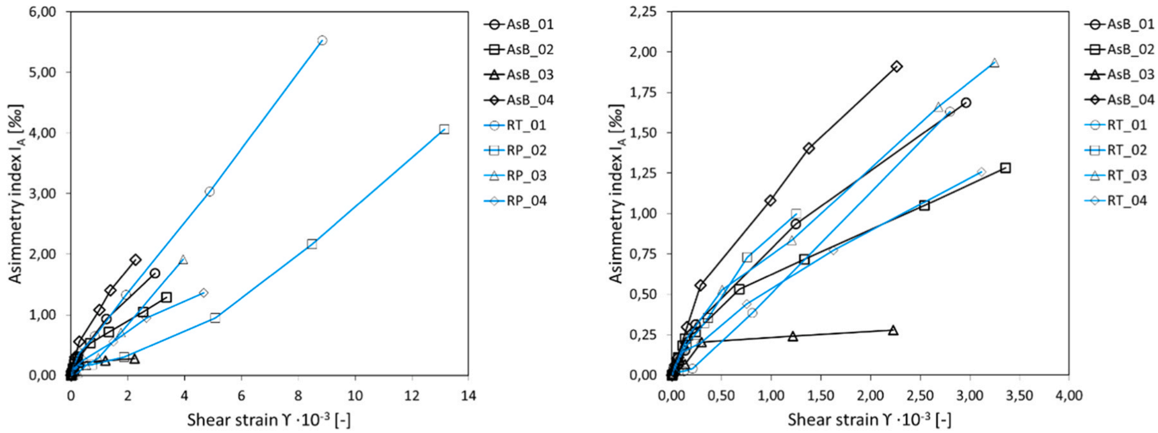

a) *RP vs AsB specimens* b) *RT vs AsB specimens*

Fig. 9. *Comparison of the experimental Asymmetry Index.*

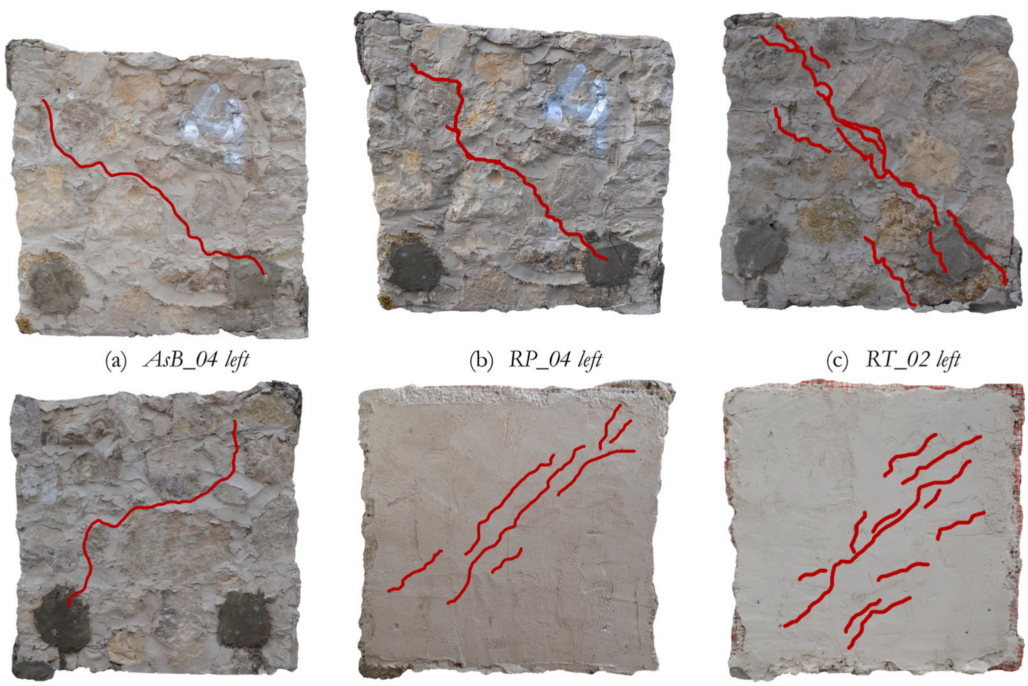

(a) *AsB_04 left* (b) *RP_04 left* (c) *RT_02 left*

(d) *AsB_04 right* (e) *RP_04 right* (f) *RT_02 right*

Fig. 10. *Failure mode of AsB_04, RP_04, and RT_02.*

rigidity that is typical of cementitious systems. From experimental observations it was confirmed that no detachment or relative slip at the matrix-to-masonry interface occurred during the initial loading stages. Because the bond remained fully effective during the elastic phase, the lateral stiffness (dowel action) of the anchors was not engaged. This behaviour aligns with experimental evidence for similar single-sided CRM systems [79,83], where mechanical anchors primarily ensured post-peak composite action rather than increasing the initial in-plane shear stiffness [38].

The experimental shear stress vs strain curves were bi-linearized using the EEEP approach proposed by ASTM E2126–19 [81], as reported in Table 6. The as-built wallettes (*AsB*) showed an average value of yield strain γ_y equal to $0.25 \cdot 10^{-3}$, with a limited non-linear descending branch reaching an average ultimate shear strain γ_u of $2.70 \cdot 10^{-3}$ based upon the adopted definition for ultimate shear strain corresponding to 10% loss of post-peak capacity. The repaired specimens (*RP*) exhibited an average yielding strain γ_y of $0.91 \cdot 10^{-3}$ that was greater than three times the value calculated for the as-built wallettes. Despite the maximum force values being similar to the values reached by the as-built wallettes, the ultimate strain values obtained for the *RP* wallettes were highly scattered, with *RP_01* and *RP_02* exhibiting ductile post-peak response while *RP_03* and *RP_04* achieved values of γ_u similar to the as-built wallettes. The dissipated energy (En_{dis}) of the *RP* wallettes was approximately 2.45 times the value measured for the *AsB* wallettes (see Table 6). The retrofitted (*RT*) wallettes exhibited shear strain values comparable to the *AsB* wallettes, reaching an average value of $\gamma_y = 0.33 \cdot 10^{-3}$ and $\gamma_u = 2.6 \cdot 10^{-3}$ respectively, although it is noted that this finding is influenced by the adopted definition for test termination and that the shear strength of the retrofitted specimens generally exceeded the shear strength of the repaired specimens at test termination, suggesting that it may be incorrect to infer that the retrofitted specimens had less strain capacity than the repaired specimens. Notably, the dissipated energy En_{dis} increased by 20% with respect to the *AsB* wallettes, demonstration that the CRM reinforcement allowed the

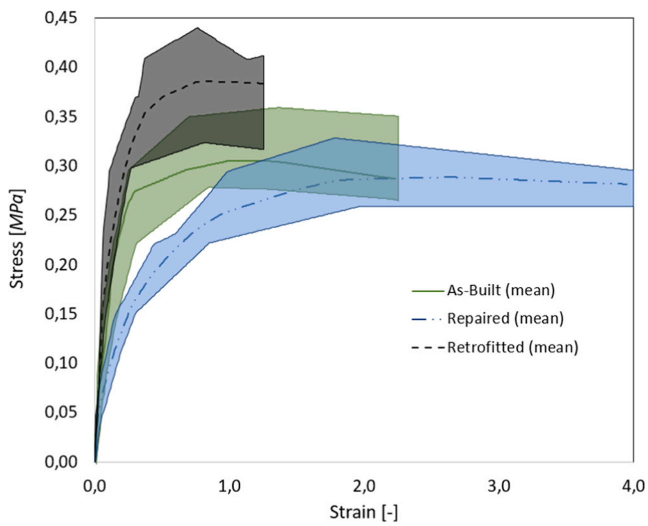

Fig. 11. Comparison of the mean experimental shear stress-strain curves. The shaded regions represent the minimum–maximum envelope of the individual experimental curves.

Table 7
Performance Ratio (PR) of the repaired (RP) and retrofitted (RT) specimens for peak shear stress (τ_{max}) and shear modulus (G_{el}).

Group	Label	$PR(\tau_{max})$	$PR(G_{el})$
Repaired	*RP_01*	1.00	0.16
	RP_02	0.75	0.26
	RP_03	1.12	0.21
	RP_04	1.06	0.49
	Average	**0.98**	**0.28**
	C.O.V.	**0.17**	**0.52**
Retrofitted	*RT_01*	1.05	1.24
	RT_02	1.43	0.87
	RT_03	1.43	0.64
	RT_04	1.38	1.36
	Average	**1.32**	**1.03**
	C.O.V.	**0.14**	**0.32**

retrofitted specimens to dissipate additional energy. Although the adopted natural hydraulic lime mortar exhibited relatively high compressive strength to ensure uniform testing conditions, such strength does not compromise compatibility with weaker historic masonry. In fact, when natural hydraulic lime mortars are employed, their intrinsic vapour permeability and deformability ensure adequate physical and mechanical compatibility with traditional lime-based substrates [84]. Therefore, the proposed CRM technique remains appropriate for the repair or strengthening of masonry originally built with low-strength mortars.

6. Comparison with codes provisions

Although the effectiveness of CRM techniques has been repeatedly demonstrated and despite high-thickness reinforced plasters being widely used to improve the seismic capacity of existing masonry buildings, there is limited information available about the design of such strengthened solutions in current codes and guidelines. Consequently, a comparison between the experimental results reported in Table 6 and the predicted values obtained using existing analytical formulations was undertaken.

As previously mentioned, design guidelines for CRM systems are currently not available in Italy and the only method available to compute the increase in the in-plane shear capacity of a CRM system is to refer to the current Italian code directives [66]. A simplified approach is suggested in NTC18 [71] and its Commentary based on empirically derived amplification coefficients to apply to strength and stiffness parameters, categorising these coefficients according to the most common existing masonry textures. For roughly squared stone panels a design coefficient of α_{NTC18}= 1.50 is suggested to amplify the URM shear capacity when a traditional ferrocement jacket is applied. The present code also considers the possibility of using this type of reinforcement applied to non-traditional materials such as lime-based mortars and fiber meshes. In addition, the provided design factors are valid for symmetrical configurations with transversal anchorages and for masonry with good-quality bed-joint mortar. NTC18 [71] allows for the possibility of using this technique in single-sided applications, reducing the amplification coefficients, but does not specify the decreased value nor the logic for how to apply a reduced value. In addition, the NTC18 amplification coefficients do not take into account several important parameters, such as the panel and reinforcement thicknesses or the mechanical proprieties of the used matrix and grid. Due to the lack of proper formulations for the strengthening method adopted in this study, the approach provided by the Italian CNR-DT 215/2018 [58] and the American ACI 549.6R-20 [57] guidelines for the design of strengthening solutions made with Fabric/Fiber Reinforced Cementitious Matrix (FRCM) are considered.

ACI 549.6R-20 [57] was prepared as a liaison between ACI Committee 549 and RILEM TC 250 Liaison Subcommittee, with the document providing both a North American (ACI) approach and a European (RILEM) approach. The North American approach incorporates ASTM standards, the International Code Council-Evaluation Services (ICC-ES) Acceptance Criteria AC434 [85], and the recommendations provided in ACI 549.4 R [57] and reflects practices commonly adopted in North America for material characterization, system qualification, and structural design of FRCM and SRG systems. Conversely, the European approach aligns with the framework provided by the European Committee for Standardization (CEN) through the EN standards and the technical recommendations from RILEM Technical Committees, and incorporates European research and practices for material and structural evaluation. In both the CNR-DT 215/2018 [58] and ACI 549.6R-20 [57] guidelines the calculation of the reinforced masonry shear strength, τ_r, is based on an additive approach where the fiber contribution, τ_f, is added

Table 8
Shear strength comparison between present experimental data and results available in the literature for single-sided CRM reinforcement systems.

Ref.	Masonry type [–]	As-built: Shear strength [MPa]	As-built: Number of specimens [–]	Reinforced: Mesh tensile strength[(1)] [kN/m]	Reinforced: Shear strength [MPa]	Reinforced: Number of specimens [–]	Effectiveness: R / AsB[(2)] [–]	Effectiveness: R - AsB[(3)] [–]
This study	Rubble dolostone	0.310	4	40	0.410	4	1.32	0.100
[83]	Rubble stone	0.200	2	79	0.294	2	1.47	0.095
[59]	Tuff	0.250	6	75	0.460	2	1.81	0.205
				53	0.390	2	1.54	0.135
[79]	Rubble limestone	0.395	3	53	0.647	6	1.64	0.252

(1)Values extrapolated from the references. If available the minimum value in the principal directions is considered. Test methods are not declared therefore values may not be fully representative for comparison.
(2)R / AsB = ratio between the experimentally observed shear strength of the reinforced configuration and that of the as-built configuration;
(3)R - AsB = shear strength increment calculated as the difference between the shear strength of the reinforced configuration and that of the as-built configuration;

to the plain masonry shear strength, τ_m, as reported in Eq. (7):

$$\tau_r = \tau_m + \tau_f \tag{7}$$

In the three considered approaches there are similar formulations proposed for the computation of the fiber contribution τ_f, differing principally in the values of the safety factors and in the assumptions made for the design parameters of the composite reinforcement.

The mechanical predictive equation for computing τ_f provided by the ACI method is reported in Eq. (8):

$$\tau_{f,ACI} = \Phi_v \cdot \frac{n \bullet A_f \bullet E_f \bullet \varepsilon_{fd}}{A_n} \tag{8}$$

Where $\Phi_v = 0.8$ is the strength reduction factor for shear-controlled failure modes, n is the number of wall sides strengthened with the composite plaster, E_f is the stiffness of the cracked composite specimen referred to the fabric cross-section, ε_{fd} is the reinforcement design tensile strain (which is, in turn, equal to the characteristic tensile strain), A_n is the net area of the panel cross section, A_f is the area of the fabric effective in shear and for the case of full coverage of the wall surface A_f is provided by Eq. (9).

$$A_f = \mathrm{MIN}(H, L) \bullet t_{fH} \tag{9}$$

where H and L are the panel height and length, and t_{fH} is the equivalent thickness of the composite reinforcement in the horizontal direction. When the FRCM system is applied to only one side of the wall the shear capacity calculated as per Eq. (8) should be multiplied by a reduction factor of 0.7. The resulting ACI strength values are reported in Table 9 with distinctions made between calculations undertaken considering design values and mean experimental values of the ultimate strain. Since mechanical properties of the actual composite system were not assessed in the study, two alternative approaches were considered. In the "Fabric" approach, the ultimate strain and the cracked modulus of elasticity of the composite were considered as equal to the corresponding properties of the mesh and based on values reported in Table 2 (as also recommended in [64], [65]).

In the "Composite" approach the mechanical properties of the composite reported in Table 3 were used in the calculations. Because in each case the calculated value of ε_{fd} exceeded the limit strain defined in the ACI method [57] to prevent excessive damage in the structural member reinforced with FRCM, a value of $\varepsilon_{fd} = \varepsilon_{lim} = 0.004$ was adopted in the calculations reported in Table 9. In the "Mean" rows the shear contribution of the reinforcement was calculated by assuming $\Phi_v = 1$.

Recognising the significant influence of the strain limit proposed in the ACI method, a modified procedure was investigated where the prescribed limit of $\varepsilon_{fd} = \varepsilon_{lim} = 0.004$ was abandoned and the strain data was instead based on experimentally derived values. In Table 10 the calculations of Table 9 are repeated, but with the mesh characteristic and mean ultimate strain data from Table 2 and the characteristic and mean composite ultimate strain data from Table 3 instead being adopted.

The design method proposed by RILEM standard to determinate the reinforcement contribution τ_f is reported in Eq. (10). This formulation is similar to the ACI approach, with a multiplicative safety factor γ_k, equal to 0.50, calibrated to account for the scatter between the theoretical and experimental increases of shear strength provided by FRCM/SRG systems.

Table 10
Modified ACI shear strength predictions (not enforcing the strain limit of 0.004) for τ_f.

Values	Tensile basis	n [-]	L [mm]	t_{fH} [mm]	E_f [MPa]	ε_{fd} [%]	τ_{f,MOD_ACI} [MPa]
Design	Fabric	1	1200	0.046	63057	1.63	0.066
	Composite	1	1200	0.046	28491	1.25	0.023
Mean	Fabric	1	1200	0.046	63057	1.94	0.098
	Composite	1	1200	0.046	28491	1.91	0.044

$$\tau_{f,RILEM} = \frac{\gamma_k \bullet n \bullet A_f \bullet E_f \bullet \varepsilon_{fd}}{A_n} \tag{10}$$

In the RILEM approach the reinforcement tensile modulus of elasticity should be assumed equal to the average value of the tensile modulus of elasticity of the fabric (see Table 2). Most significantly, the RILEM approach does not impose a limitation on the design tensile strain ε_{fd}, such that the value should be determined in accordance with Eq. (11):

$$\varepsilon_{fd} = \frac{1}{\gamma_{m,RILEM}} \bullet \min\left(\alpha_1 \bullet \varepsilon_{fb}; \frac{\varepsilon_{tk}}{\alpha_2}\right) \tag{11}$$

where ε_{fb} is the characteristic maximum tensile strain in the fabric attained in shear bond tests (see Table 4), ε_{tk} is the fabric characteristic ultimate tensile strain (see Table 2), $\gamma_{m,RILEM}$ is a partial safety factor equal to 1.50, and α_1 and α_2 are two coefficients that are calibrated by comparing experimental results with average theoretical data, equal to 1.15 and 1.25 respectively. Since the mechanical properties of the actual composite were not assessed, the parameters listed in Table 11 were calculated according to two alternative approaches. In the "Fabric" approach the calculation is based on the ultimate strain of the fabric, and the $\alpha_1 \times \varepsilon_{fb}$ term of Eq. (11) is neglected. This procedure yields values consistent with the RILEM procedure, provided that, for the tested composite system, $\alpha_1 \times \varepsilon_{fb} > \varepsilon_{tk}/\alpha_2$. In the "Composite" method, the bond parameters of the composite system were assumed as reported in Table 4. The "Design" rows in Table 11 present values calculated according to the standard RILEM procedure as per Eq. (11), while the "Mean" rows reflect the implementation of Eq. (11) using mean values of the mechanical properties along with a partial safety factor $\gamma_{m,RILEM} = 1.0$. Similarly to the ACI design method, $\tau_{f,RILEM}$ should be multiplied by a reduction factor equal to 0.70 to account for the asymmetrical application of the composite plaster.

The approach proposed by CNR-DT 215/2018 [58], presented in Eq. (12), is similar to the previously reported formulations except for the inclusion of an additional multiplicative coefficient:

$$\tau_{f,CNR} = \frac{0.5 \bullet n_f \bullet t_f \bullet l_f \bullet \alpha_t \bullet E_f \bullet \varepsilon_{fd}}{A_n} \tag{12}$$

where n_f is the number of grid layers applied on each panel side, t_f is the fabric equivalent thickness, l_f is the length of the FRCM system measured orthogonal to the shear force, α_t is a coefficient taking into account a reduced tensile strength for fibres subjected to shear (equal to 0.80), E_f is the fabric elastic modulus, ε_{fd} is the design strain of the FRCM system

Table 9
ACI shear strength predictions for τ_f.

Values	Tensile basis	n [-]	L [mm]	t_{fH} [mm]	E_f [MPa]	$\varepsilon_{fd} = \varepsilon_{lim}$ [%]	$\tau_{f,ACI}$ [MPa]
Design	Fabric	1	1200	0.046	63057	0.40	0.016
	Composite	1	1200	0.046	28491	0.40	0.007
Mean	Fabric	1	1200	0.046	63057	0.40	0.020
	Composite	1	1200	0.046	28491	0.40	0.009

Table 11
RILEM shear strength predictions for τ_f.

Values	Tensile basis	γ_k [-]	n [-]	L [mm]	t_{fH} [mm]	E_f [MPa]	$\gamma_{m,RILEM}$ [-]	ε_{fb} [%]	ε_{tk} [%]	ε_{fd} [%]	$\tau_{f,RILEM}$ [MPa]
Design	Fabric	0.5	1	1200	0.046	63057	1.5	-	0.91	0.49	0.012
	Composite	0.5	1	1200	0.046	63057	1.5	0.73	0.91	0.49	0.012
Mean	Fabric	0.5	1	1200	0.046	63057	1.0	-	1.40	1.12	0.028
	Composite	0.5	1	1200	0.046	63057	1.0	1.29	1.40	1.12	0.028

and A_n is the net area of the panel cross section. According to the CNR guidelines, the design strain ε_{fd} to be considered for in-plane shear actions is governed by the intermediate debonding failure mode, which defines the strain at failure, as given by Eq. (13):

$$\varepsilon_{fd} = \frac{\eta}{\gamma_{m,CNR}} \bullet \min\left(\alpha \bullet \varepsilon_{lim,conv}; \frac{\sigma_u}{E_f}\right) \tag{13}$$

where η is a factor that accounts for environmental conditions and the potential for material long-term degradation; σ_u is the characteristic ultimate tensile strength of the composite referred to the fabric cross section; $\varepsilon_{lim,conv}$ is the characteristic value of the ultimate strain based on bond tests (equivalent to ε_{fb} according to RILEM); and α is an amplification factor which, for the composite system with parameters listed in Table 3 and in Table 4, is equal to 1.5. Because the wallettes tested in this study were stored in a covered location and testing was completed without significant delay following the application of the reinforcement system, it was assumed that $\eta = 1$. Similar to the RILEM procedure, 2 alternative approaches were considered, obtaining the results given in Table 12.

In the "Fabric" rows, the design strain was calculated based on the ultimate tensile strength of the composite σ_u, which was assumed to be equal to the ultimate tensile strength of the mesh. The $\alpha \times \varepsilon_{lim,conv}$ term in Eq. (13) was neglected. The "Fabric" procedure is therefore consistent with the CNR guidelines if it is assumed that, for the tested composite, $\varepsilon_{tk} = \sigma_u/E_f$ and $1.5 \times \varepsilon_{lim,conv} > \varepsilon_{tk}$. In the "Composite" rows the calculations were performed assuming that the composite parameters reported in Table 3 and in Table 4 are representative of the composite used to strengthen the wallettes. The "Mean" rows report the results obtained by filling the equations with mean values of the mechanical properties in place of the characteristic values and by assuming $\gamma_{m,CNR} = 1$. The "Characteristic" rows refer to calculations carried out using the characteristic values of the mechanical properties together with $\gamma_{m,CNR} = 1.5$, as recommended by the CNR guidelines. To account for the single-sided strengthening application, and in accordance with the CNR procedure, $\tau_{f,CNR}$ was reduced by 30% in all cases.

To better interpret the data presented in Table 9, Table 10, Table 11, and Table 12 the term 'relative improvement' of the reinforced system is defined as τ_f/τ_m, where τ_m is the shear strength of the as-built (*AsB*) specimens, taken from Table 6 as $\tau_m = 0.31$ MPa. In Table 13, the theoretical shear improvements obtained from the three FRCM guidelines are reported, including the modified ACI approach shown in Table 10. According to Table 6, the mean strength of the retrofitted (*RT*) specimens was $\tau_r = 0.41$ MPa and therefore the experimentally derived relative improvement was $\tau_f/\tau_m = (0.41–0.31)/0.31 = 0.32$ or 32%. It is worth noting that this calculation is analogous to the Performance Ratio defined in Table 7, with the distinction that it focuses solely on the improvement attributable by the reinforcement system. In Table 13, the ratio between the theoretical and experimental relative improvements is shown in parentheses.

Table 13
Predicted relative improvement (τ_f/τ_m) of the FRCM guidelines and (in parentheses) comparison to the experimental relative improvement.

Values	Tensile basis	$\tau_{f,ACI}/\tau_m$ [%]	$\tau_{f,MOD\_ACI}/\tau_m$ [%]	$\tau_{f,RILEM}/\tau_m$ [%]	$\tau_{f,CNR}/\tau_m$ [%]
Design	Fabric	5.2 (16%)	21.4 (67%)	4.0 (12%)	6.0 (19%)
	Composite	2.4 (7%)	7.4 (23%)	4.0 (12%)	2.9 (9%)
Mean	Fabric	6.5 (20%)	31.8 (99%)	9.2 (29%)	9.2 (29%)
	Composite	3.0 (9%)	14.1 (44%)	9.2 (29%)	6.3 (20%)

From Table 13 it can be seen that the theoretic predictions according to ACI/RILEM/CNR significantly underestimated the level of improvement provided by the reinforcement system, in the range of 7%-40% of the measured value. While a certain degree of conservatism and solid safety margins are to be expected when referring to design values, strength predictions based on mean values should better approximate the experimental evidence. In this regard, the modified ACI method using mean fabric properties appears to be the most promising approach, as it accurately predicts the experimental value. In general, the forecast strengths using the FRCM guideline methods were similar, confirming the generally consistent approach of the three methods. As expected, the (unmodified) ACI approach provided the most conservative estimate of τ_f due to the limitation imposed on the design axial strain.

The amplification parameter $\alpha_{NTC18} = 1.50$ proposed in the Italian code [71] and its Commentary significantly overestimated the measured strength contribution for the *RT* specimens. However, this factor is associated with double-sided applications, and it is stated that the value of the parameter should be reduced for single-sided applications, but without providing a specific value. If it were to be assumed that the 50% enhancement for double-sided applications should be halved for single sided applications recognising that there is only half the amount of reinforcement provided, and if the customary factor of 0.7 is applied for a single-sided applications, then the enhancement would reduce to $0.7 \times 25\% = 17.5\%$, which would significantly underestimate the measured enhancement of 32%. The above findings indicate that further clarification of the mechanisms and factors used to select the design strain would be useful for designers, that additional advice on design capacities for single-sided applications would be helpful, and that despite the similarities existing in current FRCM guidelines, ongoing

Table 12
CNR shear strength predictions for τ_f.

Values	Tensile basis	n_f [-]	t_{fH} [mm]	l_f [mm]	α_t [-]	E_f [MPa]	$\gamma_{m,CNR}$ [-]	$\varepsilon_{lim,conv}$ [%]	σ_u [MPa]	ε_{fd} [%]	$\tau_{f,CNR}$ [MPa]
Design	Fabric	1	0.046	1200	0.80	63057	1.5		574	0.91	0.018
	Composite	1	0.046	1200	0.80	63057	1.5	0.67	425	0.45	0.009
Mean	Fabric	1	0.046	1200	0.80	63057	1.0	-	574	1.40	0.028
	Composite	1	0.046	1200	0.80	63057	1.0	0.96	603	0.96	0.019

liaison between the various code committees would be helpful to reach a uniform consensus on the appropriate composition of the governing equation for the predicted strength provided by the reinforcement.

7. Conclusions

Experimental results are reported for diagonal compression testing undertaken on four as-built (*AsB*) wallettes, four repaired (*RP*) wallettes, and four retrofitted (*RT*) wallettes to determinate the effectiveness of a specific hybrid composite reinforced mortar (*CRM*) technique that combined a natural hydraulic lime-based matrix and an alkali-resistant (*AR*) glass grid fabric applied to rubble stone masonry. A single-sided reinforcement configuration was used to mimic a common practical application. Each group of specimens was analysed in terms of failure mode and resistance, stiffness, and energy dissipation. Additionally, a comparison between the experimental results and the design provisions from FRCM guidelines and NTC18 was provided. Based on the experimental results the following conclusions are drawn:

- After a single-sided application of the CRM technique to pre-damaged (*AsB*) wallettes the original shear capacity was recovered to *97%* for the repaired (*RP*) wallettes, but because of the pre-existing cracks the shear stiffness of the repaired (*RP*) wallettes decreased to only *25%* of the as-built (*AsB*) value.
- Application of the CRM system in a single-sided configuration to undamaged (retrofitted, *RT*) wallettes resulted in an increased shear strength of *32%* with respect to the as-built (*AsB*) values, with no significant increase in shear stiffness (*3%* increase).
- The energy dissipation of CRM reinforced wallettes increased by *20%* for the retrofitted (*RT*) wallettes and by *145%* for the repaired (*RP*) wallettes.
- An Asymmetry Index (I_A) was used to identify the influence of the single-sided application of the CRM system. Similar behaviour was measured between the as-built (*AsB*) wallettes and both the repaired (*RP*) and retrofitted (*RT*) wallettes, suggesting that a single-sided application is of little concern when considering possible asymmetric effects. The single-sided application has reduced strength enhancement when compared to a double-sided application, but has greater advantage in terms of aesthetics and practicality.
- The as-built (*AsB*) wallettes failed due to a single main diagonal crack oriented along the compressed diagonal at the interface between the stone units and bed-joint mortar. When the CRM reinforcement was applied the repaired (*RP*) wallettes and the retrofitted (*RT*) wallettes exhibited a more distributed cracking pattern. The use of mechanical anchorages prevented premature detachment or grid fabric rupture of the CRM system.
- The selection of the design strain to be used in the FRCM formulations significantly influences the predicted capacities. In the ACI formulation the prescribed upper limit value of the design strain of 0.004 was substantially below the values measured from experimental testing in this study, resulting in significant conservatism.
- The simplified design approach proposed by NTC18 overestimated the shear strength increase reached by the strengthened samples, although it is recognised that this parameter is intended for use in double-sided applications.

From the above findings it was concluded that additional clarification regarding the mechanisms and factors used to select the design strain would be useful for designers and that additional advice on design capacities for single-sided applications would be helpful.

CRediT authorship contribution statement

Jason Ingham: Writing – review & editing, Writing – original draft, Formal analysis. **Ivan Giongo:** Writing – review & editing, Supervision, Resources, Project administration, Investigation, Funding acquisition. **Giovanni Sommacal:** Writing – original draft, Investigation, Formal analysis, Data curation. **Ermes Rizzi:** Writing – review & editing, Writing – original draft, Investigation, Formal analysis, Data curation, Conceptualization.

Declaration of Competing Interest

The authors declare the following financial interests/personal relationships which may be considered as potential competing interests: Ivan Giongo reports equipment, drugs, or supplies was provided by Gruppo Miniera San Romedio and Biemme Srl. Ermes Rizzi reports a relationship with Gruppo Miniera San Romedio that includes: consulting or advisory. If there are other authors, they declare that they have no known competing financial interests or personal relationships that could have appeared to influence the work reported in this paper.

Acknowledgements

Gruppo Miniera San Romedio - HD System, Ville d'Anaunia (TN) provided the bedding mortar and the hydraulic lime mortar used to provide the reinforcement matrix, and Biemme S.r.l., Lucrezia di Cartoceto (Pu) provided the AR glass grid. The authors gratefully thank both suppliers for their products.

Data Availability

Data will be made available on request.

References

[1] K.S. Jagadish, S. Raghunath, K.S. Nanjunda Rao, Behaviour of masonry structures during the Bhuj earthquake of January 2001, J. Earth Syst. Sci. 112 (2003) 431–440.
[2] G. Brandonisio, G. Lucibello, E. Mele, A. De Luca, Damage and performance evaluation of masonry churches in the 2009 L'Aquila earthquake, Eng. Fail. Anal. 34 (2013) 693–714.
[3] D. Dizhur, N. Ismail, C. Knox, R. Lumantarna, J.M. Ingham, Performance of unreinforced and retrofitted masonry buildings during the 2010 Darfield earthquake, Bull. N. Z. Soc. Earthq. Eng. 43 (4) (2010) 321–339.
[4] L. Moon, D. Dizhur, I. Senaldi, H. Derakhshan, M. Griffith, G. Magenes, J. Ingham, The demise of the URM building stock in Christchurch during the 2010–2011 Canterbury earthquake sequence, Earthq. Spectra 30 (1) (2014) 253–276.
[5] A. Penna, P. Morandi, M. Rota, C.F. Manzini, F. Da Porto, G. Magenes, Performance of masonry buildings during the Emilia 2012 earthquake, Bull. Earthq. Eng. 12 (2014) 2255–2273.
[6] G. Vlachakis, E. Vlachaki, P.B. Lourenço, Learning from failure: Damage and failure of masonry structures, after the 2017 Lesvos earthquake (Greece), Eng. Fail. Anal. 117 (2020) 104803.
[7] T.M. Ferreira, A.A. Costa, A. Costa, Analysis of the out-of-plane seismic behavior of unreinforced masonry: A literature review, Int. J. Archit. Herit. 9 (8) (2015) 949–972.
[8] E. Mustafaraj, Y. Yardim, In-plane shear strengthening of unreinforced masonry walls using GFRP jacketing, Period. Polytech. Civ. Eng. 62 (2) (2018) 330–336.
[9] El Gawady, M., Lestuzzi, P., & Badoux, M. (2004, July). A review of conventional seismic retrofitting techniques for URM. *13th International Brick and Block Masonry Conference* (Vol. 4, No. 7). Amsterdam.
[10] S. Churilov, E. Dumova-Jovanoska, In-plane shear behaviour of unreinforced and jacketed brick masonry walls, Soil Dyn. Earthq. Eng. 50 (2013) 85–105.
[11] Y. Yardim, O. Lalaj, Shear strengthening of unreinforced masonry wall with different fiber reinforced mortar jacketing, Constr. Build. Mater. 102 (2016) 149–154.
[12] P.E. Mezrea, I.A. Yilmaz, M. Ispir, E. Binbir, I.E. Bal, A. Ilki, External jacketing of unreinforced historical masonry piers with open-grid basalt-reinforced mortar, J. Compos. Constr. 21 (3) (2017) 04016110.
[13] A.M. Reinhorn, S.P. Prawel, Z.H. Jia, Experimental study of ferrocement as a seismic retrofit material for masonry walls, J. Ferrocem. 15 (3) (1985) 247–260.
[14] M. Ashraf, A.N. Khan, A. Naseer, Q. Ali, B. Alam, Seismic behavior of unreinforced and confined brick masonry walls before and after ferrocement overlay retrofitting, Int. J. Archit. Herit. 6 (6) (2012) 665–688.
[15] R. Xin, P. Ma, Experimental investigation on the in-plane seismic performance of damaged masonry walls repaired with grout-injected ferrocement overlay, Constr. Build. Mater. 282 (2021) 122565.
[16] Ministero dei Lavori Pubblici (1981). Circolare 30 luglio 1981 N. 21745 - Istruzioni per l'applicazione della norma tecnica per la riparazione ed il rafforzamento degli edifici danneggiati dal sisma.

[17] Critical review of retrofitting and reinforcement techniques related to possible failure. Deliverable 3.2, N. Integr. Knowl. Based Approaches Prot. Cult. Herit. Earthq. -Induc. risk (NIKER (2010).
[18] T.C. Triantafillou, Strengthening of masonry structures using epoxy-bonded FRP laminates, J. Compos. Constr. 2 (2) (1998) 96–104.
[19] D. Ungureanu, N. Tăranu, D.A. Ghiga, D.N. Isopescu, P. Mihai, R. Cozmanciuc, Diagonal Tensile Test on Masonry Panels Strengthened with Textile-Reinforced Mortar, Materials 14 (22) (2021) 7021.
[20] N. Gattesco, I. Boem, Experimental and analytical study to evaluate the effectiveness of an in-plane reinforcement for masonry walls using GFRP meshes, Constr. Build. Mater. 88 (2015) 94–104.
[21] A. Borri, M. Corradi, R. Sisti, C. Buratti, E. Belloni, E. Moretti, Masonry wall panels retrofitted with thermal-insulating GFRP-reinforced jacketing, Mater. Struct. 49 (2016) 3957–3968.
[22] H. Mahmood, J.M. Ingham, Diagonal compression testing of FRP-retrofitted unreinforced clay brick masonry wallettes, J. Compos. Constr. 15 (5) (2011) 810–820.
[23] Servizio Tecnico Centrale, S.T.C. (2019). Linea Guida per la identificaizone, la qualificazione ed il controllo di accettazione di compositi fibrorinforzati a matrice polimerica (FRP) da utilizzarsi per il consolidamento strutturale di costruzioni esistenti, Consiglio Superiore dei Lavori Pubblici. Rome, Italy.
[24] CNR-DT 200 R1/2013, Istruzioni per la progettazione, l'esecuzione ed il controllo di interventi di consolidamento statico mediante l'utilizzo di compositi fibrorinforzati, Consiglio Nazionale delle Ricerche, 2013.
[25] ACI 440.2R-17, Guide for the Design and Construction of Externally Bonded FRP Systems for Strengthening Concrete Structures, American Concrete Institute, 2017.
[26] M.R. Ehsani, H. Saadatmanesh, A. Al-Saidy, Shear behavior of URM retrofitted with FRP overlays, J. Compos. Constr. 1 (1) (1997) 17–25.
[27] M.R. Valluzzi, D. Tinazzi, C. Modena, Shear behavior of masonry panels strengthened by FRP laminates, Constr. Build. Mater. 16 (7) (2002) 409–416.
[28] S. Grando, M.R. Valluzzi, J.G. Tumialan, A. Nanni, Shear strengthening of URM clay walls with FRP systems, Fibre-Reinf. Polym. Reinf. Concr. Struct. 2 (2003) 1229–1238.
[29] P. Roca, G. Araiza, Shear response of brick masonry small assemblages strengthened with bonded FRP laminates for in-plane reinforcement, Constr. Build. Mater. 24 (8) (2010) 1372–1384.
[30] D.V. Oliveira, I. Basilio, P.B. Lourenço, Experimental bond behavior of FRP sheets glued on brick masonry, J. Compos. Constr. 15 (1) (2011) 32–41.
[31] N. Ismail, J.M. Ingham, Polymer textiles as a retrofit material for masonry walls, Proc. Inst. Civ. Eng. -Struct. Build. 167 (1) (2014) 15–25.
[32] G. De Felice, S. De Santis, L. Garmendia, B. Ghiassi, P. Larrinaga, P.B. Lourenço, D. V. Oliveira, F. Paolacci, C.G. Papanicolaou, Mortar-based systems for externally bonded strengthening of masonry, Mater. Struct. 47 (2014) 2021–2037.
[33] M. Vailati, M. Mercuri, A. Gregori, One-head masonry panels reinforced with industrial-waste fiber reinforced mortar: Investigating the effect of bed joints and coating reinforcement in the diagonal compressive behavior, Structures 63 (2024) 106474.
[34] T.A. Pringopoulos, A.K. Thomoglou, J.G. Fantidis, A.A. Thysiadou, Z.S. Metaxa, Advanced lime mortars for historical architectural structures, Eng. Proc. 70 (2024) 58.
[35] F.G. Carozzi, C. Poggi, Mechanical properties and debonding strength of Fabric Reinforced Cementitious Matrix (FRCM) systems for masonry strengthening, Composites Part B Engineering 70 (2015) 215–230.
[36] F.G. Carozzi, A. Bellini, T. D'Antino, G. De Felice, F. Focacci, Ł. Hojdys, L. Laghi, E. Lanoye, F. Micelli, M. Panizza, C. Poggi, Experimental investigation of tensile and bond properties of Carbon-FRCM composites for strengthening masonry elements, Composites Part B Engineering 128 (2017) 100–119.
[37] L.A.S. Kouris, T.C. Triantafillou, State-of-the-art on strengthening of masonry structures with textile reinforced mortar (TRM), Constr. Build. Mater. 188 (2018) 1221–1233.
[38] M. Angiolilli, A. Gregori, M. Pathirage, G. Cusatis, Fiber Reinforced Cementitious Matrix (FRCM) for strengthening historical stone masonry structures: experiments and computations, Eng. Struct. 224 (2020) 111102.
[39] T. D'Antino, F.G. Carozzi, C. Poggi, Diagonal shear behavior of historic walls strengthened with composite reinforced mortar (CRM), Mater. Struct. 52 (6) (2019) 114.
[40] M. Shabdin, M. Zargaran, N.K.A. Attari, Experimental diagonal tension (shear) test of Un-Reinforced Masonry (URM) walls strengthened with textile reinforced mortar (TRM), Constr. Build. Mater. 164 (2018) 704–715.
[41] N. Ismail, J.M. Ingham, In-plane and out-of-plane testing of unreinforced masonry walls strengthened using polymer textile reinforced mortar, Eng. Struct. 118 (2016) 167–177.
[42] S. De Santis, F.G. Carozzi, G. De Felice, C. Poggi, Test methods for textile reinforced mortar systems, Composites Part B Engineering 127 (2017) 121–132.
[43] M. Giaretton, D. Dizhur, E. Garbin, J.M. Ingham, F. Da Porto, In-plane strengthening of clay brick and block masonry walls using textile-reinforced mortar, J. Compos. Constr. 22 (5) (2018) 04018028.
[44] S. Yin, S. Cheng, L. Jing, Z. Huang, Shear behavior of brick masonry walls strengthened with textile-reinforced concrete, J. Compos. Constr. 25 (3) (2021) 04021017.
[45] Y. Shiping, W. Boxue, Z. Chenxue, L. Shuang, Bond performance between textile reinforced concrete (TRC) and brick masonry under conventional environment, in: Structures, 36, Elsevier, 2022, pp. 392–403.
[46] A. Borri, G. Castori, M. Corradi, Shear behavior of masonry panels strengthened by high strength steel cords, Constr. Build. Mater. 25 (2) (2011) 494–503.
[47] L. Facconi, S. Lucchini, F. Minelli, G. Plizzari, Analytical model for the in-plane resistance of masonry walls retrofitted with steel fiber reinforced mortar coating, Eng. Struct. 275 (2023) 115232, https://doi.org/10.1016/j.engstruct.2022.11523.
[48] M. Mercuri, M. Vailati, A. Gregori, Two-heads brick masonry walls strengthened by basalt and glass chopped fiber mortar: Effect of bed joints and coating reinforcements, Structures 64 (2024) 106530.
[49] Mingke, D., Zhifang, D., Experimental investigation on tensile behavior of carbon textile reinforced mortar (TRM) added with short polyvinyl alcohol (PVA) fibers.
[50] M. Deng, Z. Dong, C. Zhang, Experimental investigation on tensile behavior of carbon textile reinforced mortar (TRM) added with short polyvinyl alcohol (PVA) fibers, Constr. Build. Mater. 235 (2020) 117801, https://doi.org/10.1016/j.conbuildmat.2019.117801.
[51] Z. Dong, M. Deng, C. Zhang, Y. Zhang, H. Sun, Tensile behavior of glass textile reinforced mortar (TRM) added with short PVA fibers, Constr. Build. Mater. 260 (2020) 119897, https://doi.org/10.1016/j.conbuildmat.2020.119897.
[52] M. Angiolilli, A. Gregori, S. Cattari, Performance of Fiber Reinforced Mortar coating for irregular stone masonry: Experimental and analytical investigations, Constr. Build. Mater. 294 (2021) 123508.
[53] A. Prota, G. Marcari, G. Fabbrocino, G. Manfredi, C. Aldea, Experimental in-plane behavior of tuff masonry strengthened with cementitious matrix-grid composites, J. Compos. Constr. 10 (3) (2006) 223–233.
[54] X. Zhang, W. He, Y. Zhang, C. Chen, X. Wu, Tensile Behavior of Basalt-Fiber-Grid-Reinforced Mortar before and after Exposure to Elevated Temperature, Buildings 12 (12) (2022) 2269, https://doi.org/10.3390/buildings12122269.
[55] Servizio Tecnico Centrale, S.T.C. (2018). Linea Guida per la identificazione, la qualificazione ed il controllo diaccettazione di compositi fibrorinforzati a matrice inorganica (FRCM) da utilizzarsi per il consolidamento strutturale di costruzioni esistenti, Consiglio Superiore dei Lavori Pubblici. Rome, Italy.
[56] European Organisation for Technical Assessment (EOTA) – Externally-bonded composite systems with inorganic matrix for strengthening of concrete and masonry structures – EAD 340275–00-0104, January 2018.
[57] ACI 549.6R-20 (2020). Guide to design and construction of externally bonded fabric-reinforced cementitious matrix (FRCM) and steel-reinforced grout (SRG) systems for repair and strengthening masonry structures. American Concrete Institute, 2020.
[58] CNR-DT 215/2018, Istruzioni per la progettazione, l'esecuzione ed il controllo di interventi di consolidamento statico mediante l'utilizzo di compositi fibrorinforzati a matrice inorganica, Consiglio Nazionale delle Ricerche, 2019.
[59] M. Del Zoppo, M. Di Ludovico, A. Balsamo, A. Prota, In-plane shear capacity of tuff masonry walls with traditional and innovative composite reinforced mortars (CRM), Constr. Build. Mater. 210 (2019) 289–300.
[60] S. de Santis, G. de Felice, G.L. Di Noia, P. Meriggi, M. Volpe, Shake table tests on a masonry structure retrofitted with composite reinforced mortar, Key Eng. Mater. 817 (2019) 342–349.
[61] T. D'Antino, F.G. Carozzi, C. Poggi, Diagonal shear behavior of historic walls strengthened with composite reinforced mortar (CRM), Mater. Struct. 52 (6) (2019) 114.
[62] S. De Santis, G. de Felice, Shake table tests on a tuff masonry structure strengthened with composite reinforced mortar, Compos. Struct. 275 (2021) 114508.
[63] N. Gattesco, E. Rizzi, I. Boem, L. Facconi, F. Minelli, A. Dudine, M. Gams, Full-scale cyclic tests on a stone masonry building to investigate the effectiveness of a one-side application of the composite reinforced mortar system, Eng. Struct. 296 (2023) 116967.
[64] Servizio Tecnico Centrale, STC (2019). Linea Guida per la identificazione, la qualificazione ed il controllo di accettazione dei sistemi a rete preformata in materiali compositi fibrorinforzati a matrice polimerica da utilizzarsi per il consolidamento strutturale di costruzioni esistenti con la tecnica dell'intonaco armato CRM (Composite Reinforced Mortar). Rome, Italy.
[65] European Organisation for Technical Assessment (EOTA) – CRM (Composite Reinforced Mortar) systems for strengthening concrete and masonry structures – EAD 340392–00-0104, November 2018.
[66] Circolare 21 gennaio 2019, Istruzioni per l'applicazione dell'«Aggiornamento delle "Norme tecniche per le costruzioni"» di cui al decreto ministeriale 17 gennaio 2018, Ministero delle Infrastrutture e dei Trasporti, 2019.
[67] A.K. Thomoglou, T.C. Rousakis, D.V., A. Achillopoulou, A.I. Karabinis, Ultim. Shear Strength Predict. Model unreinforced Mason. Retrofit. Extern. Text. Reinf. Mortar Struct. 53 (2020) 1–17.
[68] N. Trochoutsou, M. di Benedetti, K. Pilakoutas, M. Guadagnini, In-plane cyclic performance of masonry walls retrofitted with flax textile-reinforced mortar overlays, Asce J. Compos. Struct. (2022).
[69] M. Del Zoppo, M. Di Ludovico, A. Balsamo, A. Prota, Diagonal compression testing of masonry panels with irregular texture strengthened with inorganic composites, Mater. Struct. 53 (2020) 1–17.
[70] ASTM E519/E519M-15, Standard test method for diagonal tension (shear) in masonry assemblages, American Society for Testing and Materials, 2020.
[71] D. M. 17 gennaio 2018, Aggiornamento delle «Norme tecniche per le costruzioni», Ministero delle Infrastrutture e dei Trasporti, 2018.
[72] ASTM C568/C568M-15, Standard specification for limestone dimension stone, American Society for Testing and Materials, 2015.
[73] ASTM C170/C170M-17, Standard test method for compressive strength of dimension stone, American Society for Testing and Materials, 2017.
[74] L.I.G. de Vallejo, Geoingegneria, Pearson Italia Spa, 2004.
[75] EN 998–2:2016, Specification for mortar for masonry - Part 2: Masonry mortar, European Committee for Standardization, 2016.

[76] EN 1015–11:2019, Methods of test for mortar for masonry – Part 11: Determination of flexural and compressive strength of hardened mortar, European Committee for Standardization, 2019.
[77] EN 1990:2002+A1:2005, Eurocode – Basis of Structural Design, European Committee for Standardization, 2002.
[78] A. Drougkas, P. Roca, C. Molins, Compressive strength and elasticity of pure lime mortar masonry, Mater. Struct. 49 (2016) 983–999.
[79] Del Zoppo, M., Maddaloni, G., Di Ludovico, M., Balsamo, A., Prota, A. (2019). FRCM for the in-plane shear strengthening of masonry panels with irregular texture. Proceedings of the XVIII ANIDIS Conference, Ascoli Piceno, Italy.
[80] M. Del Zoppo, M. Di Ludovico, A. Prota, Analysis of FRCM and CRM parameters for the in-plane shear strengthening of different URM types, Composites Part B Engineering 171 (2019) 20–33.
[81] ASTM E2126-19 (2019). Standard test methods for cyclic (reversed) load test for shear resistance elements of the lateral force resisting systems buildings, American Society for Testing and Materials.
[82] FprEN 1998-3:2025, Eurocode 8 - Design of structures for earthquake resistance - Part 3: Assessment and retrofitting of buildings and bridges, European Committee for Standardization, 2025.
[83] N. Gattesco, A. Dudine, Effectiveness of masonry strengthening technique made with a GFRP-mesh-reinforced mortar coating, in: Masonry, 11, Alinea Digitaldruck GmbH, 2010.
[84] A. Borri, G. Castori, M. Corradi, E. Speranzini, Shear behavior of unreinforced and reinforced masonry panels subjected to in situ diagonal compression tests, Constr. Build. Mater. 25 (2011) 4403–4414.
[85] ICC Evaluation Services (2016). ICC-ES Acceptance criteria for masonry and concrete strengthening using Fibre-Reinforced Cementitious Matrix (FRCM) and Steel Reinforced Grout (SRG) composite systems, AC434, ICC Evaluation Services Inc., Los Angeles, CA, June.